Constructing gapless spin liquid state for the spin-$1/2$ $J_1 - J_2$ Heisenberg model on a square lattice

Ling Wang,[1,2] Didier Poilblanc,[3] Zheng-Cheng Gu,[2] Xiao-Gang Wen,[4,5,6] and Frank Verstraete[1]

[1]*Vienna Center for Quantum Science and Technology, Faculty of Physics,*
University of Vienna, Boltzmanngasse 5, 1090 Vienna, Austria
[2]*Institute for Quantum Information and Matter,*
California Institute of Technology, Pasadena, California 91125, USA
[3]*Laboratoire de Physique Théorique, C.N.R.S. and Université de Toulouse, 31062 Toulouse, France*
[4]*Perimeter Institute for Theoretical Physics, 31 Caroline St N, Waterloo, ON N2L 2Y5, Canada*
[5]*Department of Physics, Massachusetts Institute of Technology, Cambridge, Massachusetts 02139, USA*
[6]*Institute for Advanced Study, Tsinghua University, Beijing, 100084, P. R. China*
(Dated: February 7, 2013)

We construct a class of projected entangled pair states (PEPS) which is exactly the resonating valence bond (RVB) wavefunctions endowed with both short range and long range valence bonds. With an energetically preferred RVB pattern, the wavefunction is simplified to live in a one parameter variational space. We tune this variational parameter to minimize the energy for the frustrated spin $1/2$ $J_1 - J_2$ antiferromagnetic Heisenberg model on the square lattice. Taking a cylindrical geometry, we are able to construct four topological sectors with even or odd number of fluxes penetrating the cylinder and even or odd number of spinons on the boundary. The energy splitting in different topological sectors is exponentially small with the cylinder perimeter. We find a power law decay of the dimer correlation function on a torus, and a $\ln L$ correction to the entanglement entropy, indicating a gapless spin liquid phase at the optimum parameter.

Introduction – Resonant valence bond (RVB) states, which were first proposed by Anderson [1] to describe a possible ground state for the $S = 1/2$ antiferromagnetic Heisenberg model on a triangular lattice, and later to explain the possible mechanism of high-T_c cuprates [2, 3], provide us a rich tool box to construct the so called spin liquid states. Rokhsar Kivelson (RK) wavefunction [4], which is an equal weight superposition of nearest neighbor (NN) dimer coverings, is a critical spin liquid state [5] on square lattice; whereas a gaped $\mathbb{Z}_2$ spin liquid state on kagome and triangular lattice [6, 7]. The equal weight superposition of the NN RVB state on square lattice was shown to be critical [8, 9]. Several numerical work [10–13] have demonstrated that the equal weight NN RVB states on the kagome and triangular lattices are $\mathbb{Z}_2$ spin liquid states.

Recently numerical breakthroughs claimed a spin liquid ground state for the Kagome Heisenberg model [14, 15] and the frustrated spin $1/2$ $J_1 - J_2$ antiferromagnetic (AF) Heisenberg model on the square lattice [16, 17]. However, these work did not give direct access to the topological nature of the spin liquid states, therefore, a simple variational wavefunction approach is highly desirable. Although the variational energy of the NN RVB state on the kagome lattice [11, 13] is still higher than the energy obtained via the density matrix renormalization group (DMRG) method [14], the topological nature is well understood within the formalism of the projected entangled pair states (PEPSs) [11]. On the other hand, from a projective wavefunction [18] approach supplemented by a projective symmetry group (PSG) anal-

ysis all possible spin-liquid states on the triangular [19], Kagome [19–22] and Honeycomb [23] lattices have been obtained and classified but, for all lattices, the energetically favorable states are believed to involve longer range RVB. As a result, it is natural to think that a general RVB state within the PEPS formalism is a more practical variational wavefunction, where one can gain simultaneously an optimized energy *and* a comprehensive picture of the topological nature.

In this paper, we introduce a general RVB state written as a $D = 3$ PEPS, different from Ref. [10, 11], i.e. it includes valence bonds of all length (although with a bond amplitude decaying exponentially fast with the bond length). With a properly chosen singlet sign convention that meets all lattice symmetries on the square lattice, we minimize the energy of the spin $1/2$ $J_1 - J_2$ AF Heisenberg model at $J_2 = 0.5J_1$ against a single variational parameter c governing the decay amplitude of the long range valence bonds. The idea is therefore to introduce a simple yet competing wavefunction that enables us to fully understand the topological properties of the ground state of the frustrated magnets.

RVB states in PEPS formalism – The equal weight superposition of the NN RVB states can be constructed using a PEPS with bond dimension $D = 3$ as following: each physical site has 4 virtual spins attached, each of which spans a virtual dimension of spin $1/2 \oplus 0$. From the bond point of view, every pair of the NN virtual spins is projected to a block diagonal virtual spin singlet state:

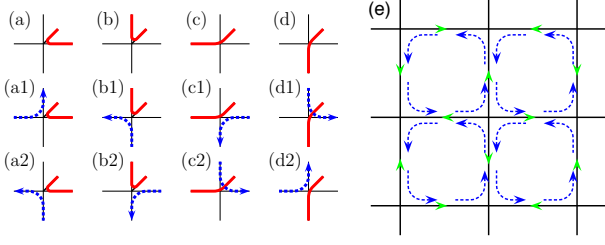$$|\mathcal{S}\rangle = |01\rangle - |10\rangle + |22\rangle, \qquad (1)$$

FIG. 1: (a-d) Red thick lines denote mappings of a virtual spin 1/2 to a physical spin 1/2, the blue dash lines represent the singlet pairings of two virtual spin-1/2s, and the black thin lines represent the virtual spin 0 states. (e) The local sign convention for the bond singlets (in green arrows) and the corner singlets (in blue arrows).

FIG. 2: (a) The NNN singlet (s_1, s_2) pairs through 2 bond singlets and 1 corner singlet via 2 paths, which cancel each other. (b) The next allowed AB sublattice pairing (s_1, s_2) through 3 bond singlets and 2 corner singlets. (c) The weight distribution in the Liang-Doucot-Anderson picture with a linear color scale for a 8×8 torus at $c = 0.35$. $h(dx, dy)$ is the weight of a singlet at separation (dx, dy), where $h(1, 0) = 1$. The plotted color scale takes the square root of $h(dx, dy)$ to magnify the weight of the long range singlet.

here the virtual indices "0,1" span the subspace of spin 1/2 and virtual index "2" spans the subspace of spin 0. At the physical site, a projector enforces one of the virtual spins with its spin 1/2 subspace to be mapped to the physical spin 1/2 state and the rest of virtual spins to stay in the spin 0 subspace, *i.e.* the "2" state,

$$\mathcal{P}_1 = \sum_{k=1}^{4} (| \uparrow \rangle \langle 0|_k + | \downarrow \rangle \langle 1|_k) \otimes \langle 222|_{/k}, \qquad (2)$$

here subscript "/k" stands for all except k. This PEPS, by contracting the virtual index of each $\mathcal{S}$ at the bond and each $\mathcal{P}_1$ at the vertex, represents exactly the equal weight NN RVB states.

To allow long distance singlet pairings, we need spins to teleportate: enforcing a singlet between site i and j that are already paired in singlets (s_1, i) and (s_2, j) will generate a singlet pair (s_1, s_2). The following projector realizes spin teleportation without increasing the bond dimension,

$$\mathcal{P}_2 = \sum_{i \neq j \neq k \neq l} (| \uparrow \rangle \langle 0|_i + | \downarrow \rangle \langle 1|_i) \otimes \langle 2|_j \otimes \langle \epsilon|_{kl}, \qquad (3)$$

here $|\epsilon\rangle_{kl} \equiv |01\rangle_{kl} - |10\rangle_{kl}$, and it forces spins connected via this site by bonds k and l into a singlet. A general RVB wavefunction is a parameter c weighted combination of projectors $\mathcal{P} \equiv \mathcal{P}_1 + c\mathcal{P}_2$ at each vertex $V \equiv \{v\}$ traced out with the bond singlets $\mathcal{S}$ at each bond $B \equiv \{b\}$,

$$|\Psi\rangle_{\text{RVB}} = \prod_V \mathcal{P} \prod_B |\mathcal{S}\rangle, \qquad (4)$$

The sign convention and symmetries – Fig. 1(a-d) enumerates 4 possible $\mathcal{P}_1$ projectors and 8 $\mathcal{P}_2$ projectors at each vertex. The bond singlet $\mathcal{S}$ is chosen such that NN singlets point from sublattice A to B; the corner singlets, which plays the role of singlet teleportation, are oriented counter clockwise and preserve all lattice symmetries. The sign convention is demonstrated in Fig. 1(e).

The NNN singlet arises through two bonds singlets and one corner singlet, as in Fig. 2(a). However the weight of
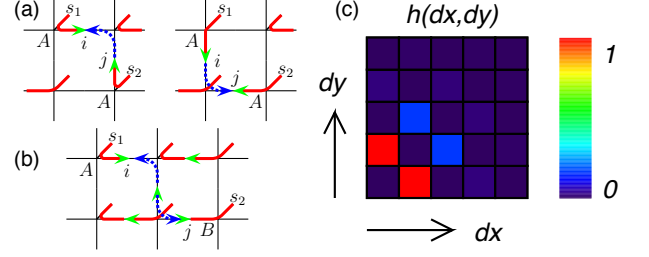
a diagonal singlet is comprised of two shortest paths of equal magnitude but opposite sign, thus the net weight of the diagonal singlet is zero. The only shortest path to build the next range AB sublattice singlet is shown in Fig. 2(b), and it consists of three bond singlets and two corners. The sign of the next range AB singlet is pointing from sublattice A to B. In general, no AA pairings survive (see Appendix) and all AB pairings point from sublattice A to B. To verify this result, we implement a Monte Carlo (MC) sampling of the singlet distribution of (4) and calculate the weight $h(dx, dy)$ defined in Ref. [18] as a function of separation. The result is presented in Fig. 2(c) and is consistent with the above analysis.

String picture – Since the RVB bonds only connect sites on different sublattices, we can view such a RVB state as a liquid state of oriented strings. Indeed, choosing a reference VB_0 configuration, any VB configuration can be viewed as a closed oriented string configuration: the RVB bonds in the VB configuration are regarded as a piece of the closed string pointing from the A to the B sublattice, while the RVB bonds in the reference VB_0 configuration are regarded as the complementary piece pointing from the B to the A sublattice.

If such a superposition of closed orientable string states indeed represent a *liquid* state of closed strings, then the entanglement entropy for a such a state in a region A has the form $S_A = aL_A - \frac{1}{2}\ln L_A + b$, where L_A is the length of the perimeter of region A. To understand such a result, we view a string as a flux line and the close-string condition implies that the flux is conserved. Therefore, the total flux going through the perimeter of A is zero. If we had ignored the flux conservation and assumed that the flux could fluctuate freely and independently, then the entanglement entropy would have an exact area-law form $S_A = aL_A$ and the typical amount of flux through the perimeter would be proportional to $\sqrt{L_A}$. So if we restrict the amount of flux through the
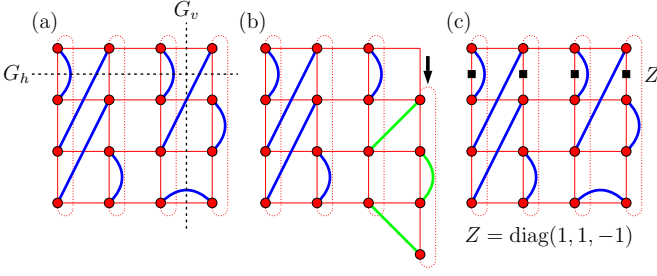
FIG. 3: (a) The parity quantum number G_v (G_h) is defined by counting the number of singlets (blue lines) modulo 2 crossed by a vertical loop (horizontal line) in dashed black line. (b) By cyclically permuting all spins in a loop winding around the cylinder, a $G_h = 1$ configuration in (a) is transformed into a $G_h = -1$ configuration in (b). Singlets in green lines are affected by the permutation operator. (c) An odd-flux state is defined by inserting operator Z on all vertical bonds crossed by a horizontal line to (4).

FIG. 4: Ground state energies (per site) computed for the $J_1 - J_2$ AF Heisenberg model at $J_2 = 0.5 J_1$, as a function of parameter c for the e/o topological sectors of (a) a cylinder ($N_v = 4, 6, 8$) with even-flux ($N_v/2$ even) or odd-flux ($N_v/2$ odd), and (b) a strip geometry with $N_v = 10, \cdots, 18$. For both cases, energy minimizes at $c = 0.35(1)$.

perimeter to be zero, the entanglement entropy will be $S_A = a L_A - \ln \sqrt{L_A} + b = a L_A - \frac{1}{2} \ln L_A + b$. The $\ln L_A$ dependence in the entanglement entropy implies that the liquid of orientable closed strings must be gapless. This property is confirmed by our numerical calculation.

Variational ground state energies at $J_2 = 0.5 J_1$ – We consider the general RVB wavefunction on a cylinder with finite cylindrical circumference N_v and infinite horizontal length $N_h = \infty$. The physical properties are determined by the eigenvector with the largest eigenvalue of the transfer matrix. Let us introduce a horizontal (vertical) parity number G_h (G_v) which is defined by counting the number of singlets modulo 2 that cross a horizontal (vertical) line joining the two boundaries of the cylinder (going around the cylinder). The two states with $G_h = \pm 1$ (+ is even and − is odd) are orthogonal to each other in the thermodynamic limit, and can be transformed from one to another by a cyclic spin permutation $\Pi_\bigcirc$ operator winding around the cylinder as illustrated in Fig. 3(a,b).

The $G_h = \pm 1$ states are not the minimally entangled states (MESs) [24]. However their superpositions,

$$|\Psi(\pm)\rangle \equiv |\Psi\rangle_{G_h=1} \pm |\Psi\rangle_{G_h=-1}, \qquad (5)$$

with a relative $\pm$ sign are. A good reason for it is that these states (5) can be written as simple PEPSs: $|\Psi(+)\rangle$ state is the state corresponding to (4), and $|\Psi(-)\rangle$ state is obtained by inserting a "vison" line to the PEPS for state $|\Psi(+)\rangle$ (by putting $Z = \mathrm{diag}(1,1,-1)$ operators on the vertical bonds crossed by a horizontal line), as in Fig. 3(c). These MESs are referred to as the even-flux ($|\Psi(+)\rangle$) states and the odd-flux ($|\Psi(-)\rangle$) states which stands for even and odd number of flux penetrating the cylinder. We will show next that these four states $|\Psi(\pm 1)\rangle_{e/o}$ are (bulk) ground states of the gapless spin liquid state.
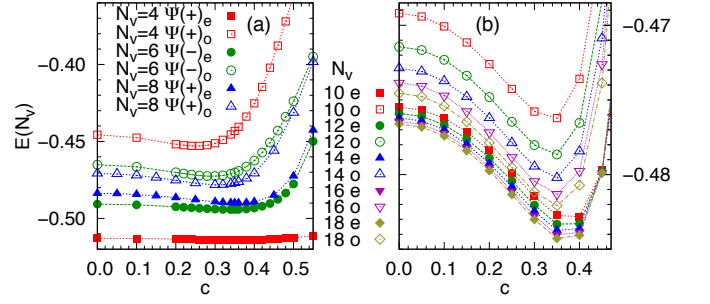
The variational energies of $|\Psi(\pm)\rangle_{e/o}$ on cylinders with finite perimeter $N_v = 4, 6, 8$ (N_v must be even, otherwise the system dimerizes) are computed *exactly* via the transfer matrix method and shown in Fig. 4(a) (an even or odd number of flux is chosen to provide the lowest energy) as a function of the variational parameter c. The best variational energy for the spin $1/2$ $J_1 - J_2$ AF Heisenberg model at $J_2 = 0.5 J_1$ is $c = 0.35(1)$ with $N_v = 4, 6, 8$. To access larger system size, we study a complementary geometry where the cylinders are cut open, with the top and bottom vertical virtual spins set to "2"s. We call them the finite (N_v) width strips. For a contractible geometry as strips, the flux parity is no longer meaningful, but the boundary parity quantum number $G_v = e(o)$ still holds. We simulate the leading eigenvectors of the transfer matrix of the strips by the matrix product states (MPS) with the same quantum number G_v in both bra and ket. The ground state energies as a function of the variational parameter c for both sectors ($|\Psi\rangle_{e/o}$) of the strips with $N_v = 10, \cdots, 18$ are presented in Fig. 4(b). The best variational energy for $J_2 = 0.5 J_1$ is at $c = 0.35$, which is in good consistency with the case of finite perimeter cylinders.

The variational energies of the even and odd sectors at the optimum parameter $c = 0.35$ as a function of inverse width $1/N_v$ are shown in Fig. 5(a,b), with cylinders of size $N_v = 4, 6, 8$ and strips up to $N_v = 36$. A linear regression is applied to the even sector of the strips and a thermodynamic limit of $E_\infty = -0.48612(2)$ is obtained. This energy is competing on the third decimal digit to the best variational estimate of $E_\infty = -0.4943(7)$ with a $D = 9$ PEPS [17], let alone the fact that here we vary only one variational parameter in a $D = 3$ PEPS. A conjecture about the ground state energies of the gapless and gaped spin liquid states is that the energy splittings between different topological sectors become exponentially small with the system size. This conjecture is verified in Fig. 5(c,d) presenting on semi-log scales the energy difference between all sectors and E_∞ for cylinders and
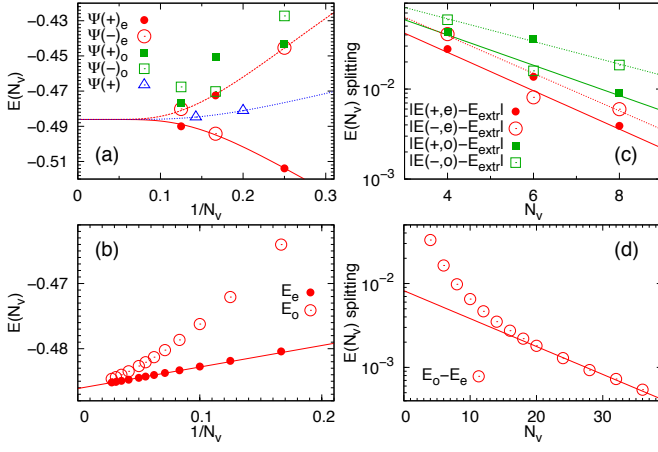
FIG. 5: Ground state energies at $c = 0.35$ as a function of $1/N_v$ for all topological sectors in (a) cylinders and (b) strips. The extrapolated ground state energy from the even sector of strips is $E_\infty = -0.48612(2)$. The ground state energy splitting between the lowest energy sector and other sectors as a function of N_v for (c) cylinders and (d) strips. The splitting vanishes exponentially with size N_v.
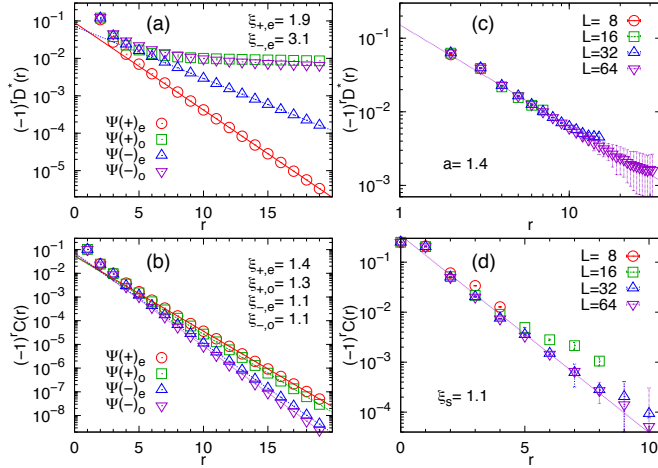

FIG. 6: The dimer (a) and the spin (b) correlation function for all topological sectors on a $N_v = 8$ cylinder at $c = 0.35$. The dimer (c) and the spin (d) correlation function on a torus with $L = 8, 16, 32, 64$ at $c = 0.35$. Note that different scales, log-log in (c) and semi-log otherwise, are used.

between the two existing energy sectors for strips.

Correlation functions and entanglement entropy – We define the spin and dimer correlation functions as the ground state expectation values $C(r) = \langle \mathbf{S_0} \cdot \mathbf{S}_r \rangle$ and $D^*(r) = \langle (\mathbf{S_0} \cdot \mathbf{S}_1)(\mathbf{S_r} \cdot \mathbf{S}_{r+1}) - (\mathbf{S_0} \cdot \mathbf{S}_1)(\mathbf{S_{r-1}} \cdot \mathbf{S}_r) \rangle$. Fig. 6(a) plots the dimer correlation functions on a cylinder with $N_v = 8$ for all topological sectors at the optimal parameter $c = 0.35$. The odd sectors have very slowly decaying dimer correlations due to an odd number of spinons sitting on the boundaries, thus the system effectively becomes an odd-width cylinder and the Majumdar-Ghosh kind of degeneracy emerges. We can eliminate
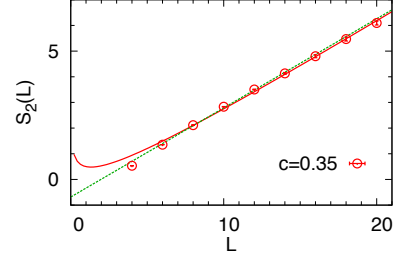

FIG. 7: Renyi entanglement entropy $S_2(L)$ for an area $L \times L$ on a torus of size $2L \times L$ with $L = 4, \cdots, 20$. The fitted red line is of form $S_2(L) = a_1 L - \frac{1}{2} \ln L + b_1$ for $L \in [6 : 18]$; the fitted green line is $S_2(L) = a_2 L + b_2$ for $L \in [6 : 14]$ and $b_2 = -0.68(1)$.

the boundary effect by setting the system on a torus and carrying a variational MC simulation for PEPSs [25]. We found the dimer correlation function exhibits a power law decay $D^*(r) \sim \frac{(-1)^r}{r^a}$ with $a = 1.4$, as shown in Fig. 6(c). In contrast, the decay of the spin correlation function for all sectors on a cylinder or on a torus remains exponential with a correlation length $\xi_s \approx 1.1$, as evidenced in Fig. 6(b,d). Fig. 7 shows the Renyi entropy $S_2(L)$ of an area $L \times L$ on a $2L \times L$ torus for size $L = 4, 6, \cdots, 20$. The fitted line of $aL - \frac{1}{2} \ln L + b$ reflects the $\ln L$ correction from the oriented string picture. The simulation is done via MC sampling of the RVB configuration [26]. Finally, we also would like to point out that the logarithmic correction is very hard to be detected on small system size. If we fit S_2 with a form $aL + b$ on small system size, we find that the constant $b = -0.68(1)$, which is very close to $-\ln 2$. Such an observation implies that the observed $-\ln 2$ constant in DMRG calculation [16] is insufficient to rule out the possibility of gapless spin liquid ground state for $J_1 - J_2$ Heisenberg model on square lattice.

Conclusion and outlook – We constructed a class of projected entangled pair states which exactly represent general RVB wavefunctions with all bond length contributions. Upon choosing an energetically preferred RVB pattern, we are able to build a one-parameter manifold of variational RVB $D = 3$ PEPSs which preserve all lattice symmetries. Minimization of the variational energy for the frustrated spin $1/2$ $J_1 - J_2$ Antiferromagnetic (AF) Heisenberg model on the square lattice yields, at $J_2 = 0.5 J_1$, an energy $E_\infty = -0.48612(2)$ per site in the thermodynamic limit. In the case of a cylinder geometry, four orthogonal topological states were identified, namely the even-flux and odd-flux states with even and odd number of spinons on the boundary. We found the dimer correlation function decays algebraically while the spin correlation function still decays exponentially. The entanglement entropy scaling reveals $\ln L$ correction to the area law. Both features point towards the gapless spin liquid nature of our constructed RVB wavefunction.

Previous valence bond MC simulations have proposed wavefunctions which violate the Marshall's sign rule by

a single negative pairing magnitude $h(2,1)$ [27, 28], however our PEPS wavefunction constructed to meet a negative $h(2,1)$ condition does not gain an optimized energy except on a very small 4×4 torus.

The PEPSs construction of the general RVB states can be applied to other bipartite and non-bipartite lattices, where the Schwinger boson spin liquid states under the projective symmetry group (PSG) analysis have been found [19–23, 29], but for which thermodynamic energies and correlation functions are still unknown due to a negative sign problem in the valence bond MC simulations. Within the PEPS formalism all of these can be easily studied. Our PEPS construction of the RVB states can be further generalized to accommodate more complicated pairing pattern which can improve further the ground state energy although possibly requiring a larger bond dimension.

[1] P. W. Anderson, Resonating valence bonds: A new kind of insulator?, Mat. Res. Bull. **8**, 153 (1973).

[2] P. W. Anderson, The resonating valence bond state in La$_2$CuO$_4$ and superconductivity, Science **235**, 1196 (1987).

[3] P. A. Lee, Naoto Nagaosa and X.-G. Wen, Doping a Mott Insulator: Physics of High Temperature Superconductivity, Rev. Mod. Phys. **78**, 17 (2006).

[4] D. S. Rokhsar and S. A. Kivelson, Superconductivity and the Quantum Hard-Core Dimer Gas, Phys. Rev. Lett. **61**, 2376 (1988).

[5] C. L. Henley, Relaxation Time for a Dimer Covering with Height Representation, J. Stat. Phys. **89**, 483 (1997).

[6] R. Moessner and S. L. Sondhi, Resonating Valence Bond Phase in the Triangular Lattice Quantum Dimer Model, Phys. Rev. Lett. **86**, 1881 (2001).

[7] G. Misguich, D. Serban and V. Pasquier, Quantum Dimer Model on the Kagome Lattice: Solvable Dimer-Liquid and Ising Gauge Theory, Phys. Rev. Lett. **89**, 137202 (2002).

[8] A. F. Albuquerque and F. Alet, Critical correlations for short-range valence-bond wavefunctions on the square lattice, Phys. Rev. B **82**, 180408R (2010).

[9] Y. Tang, A. W. Sandvik and C. L. Henley, Properties of resonating valence bond spin liquids and critical dimer models, Phys. Rev. B **84**, 174427 (2011).

[10] N. Schuch, D. Poilblanc, J. I. Cirac and D. Perez-Garcia, Resonating valence bond states in the PEPS formalism, Phys. Rev. B **86**, 115108 (2012).

[11] D. Poilblanc, N. Schuch, D. Perez-Garcia and J. I. Cirac, Topological and entanglement properties of resonating valence bond wave functions, Phys. Rev. B **86**, 014404 (2012).

[12] J. Wildeboer and A. Seidel, Correlation Functions in $SU(2)$ Invariant Resonating-Valence-Bond Spin Liquids on Nonbipartite Lattices, Phys. Rev. Lett. **109**, 147208 (2012).

[13] F. Yang and H. Yao, Frustrated Resonating Valence Bond States in Two Dimensions: Classification and Short-Range Correlations, Phys. Rev. Lett. **109**, 147209 (2012).

[14] Simeng Yan, D. A. Huse, and S. R. White, Spin-Liquid Ground State of the $S = 1/2$ Kagome Heisenberg Antiferromagnet, Science **332**, 1173 (2011).

[15] S. Depenbrock, I. P. McCulloch and U. Schollwock, Nature of the Spin Liquid Ground State of the S=1/2 Kagome Heisenberg Model , Phys. Rev. Lett. **109**, 067201 (2012).

[16] H.-C. Jiang, H. Yao and L. Balents, Spin liquid ground state of the spin-1/2 square $J_1 - J_2$ Heisenberg model, Phys. Rev. B **86**, 024424 (2012).

[17] L. Wang, Z.-C. Gu, F. Verstraete and X.-G. Wen, Spin-liquid phase in spin-1/2 square $J_1 - J_2$ Heisenberg model: A tensor product state approach , (2011), arXiv:1112.3331 (unpublished).

[18] S. Liang, B. Doucot and P. W. Anderson, Some New Variational Resonating-Valence-Bond-Type Wave Functions for the Spin-$\frac{1}{2}$ Antiferromagnetic Heisenberg Model on Square Lattice, Phys. Rev. Lett. **61**, 365 (1988).

[19] F. Wang and A. Vishwanath, Spin-liquid states on the triangular and Kagome lattices: A projective-symmetry-group analysis of Schwinger boson states, Phys. Rev. B **74**, 174423 (2006).

[20] Y. Ran, M. Hermele, P. A. Lee and X.-G. Wen, Projected-Wave-Function Study of the Spin 1/2 Heisenberg Model on Kagome Lattice, Phys. Rev. Lett. **98**, 117205 (2007).

[21] T. Tay and O. I. Motrunich, Variational study of $J_1 - J_2$ Heisenberg model on Kagome lattice using projective Schwinger-boson wave functions, Phys. Rev. B **84**, 020404R (2011).

[22] T. Tay and O. I. Motrunich, Sign structures for short-range RVB states on small Kagome clusters, Phys. Rev. B **84**, 193102 (2011).

[23] F. Wang, Schwinger boson mean field theories of spin liquid states on a honeycomb lattice: Projective symmetry group analysis and critical field theory, Phys. Rev. B **82**, 024419 (2010).

[24] Y. Zhang, T. Grover, A. Turner, M. Oshikawa and A. Vishwanath, Quasi-particle Statistics and Braiding from Ground State Entanglement, Phys. Rev. B **85**, 235151 (2012).

[25] L. Wang, I. Pizorn and F. Verstraete, Monte Carlo simulation with tensor network states, Phys. Rev. B **83**, 134421 (2011).

[26] M. B. Hastings, I. Gonzalez, A. B. Kallin and R. G. Melko, Measuring Renyi Entanglement Entropy in Quantum Monte Carlo simulations, Phys. Rev. Lett.
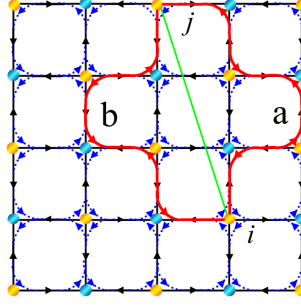
FIG. 8: (Color online) For any teleportation path contributing to the AA (BB) pairing, there always exists a dual teleportation path with opposite sign. Therefore the AA (BB) pairing amplitudes are exactly zero in $|\Psi\rangle_{\mathrm{RVB}}$.

104, 157201 (2010).

[27] J. Lou and A. W. Sandvik, Variational ground states of two-dimensional antiferromagnets in the valence bond basis, Phys. Rev. B **76**, 104432 (2007).

[28] X. Zhang and K. S. D. Beach, Resonating valence bond trial wavefunctions with both static and dynamically determined Marshall sign structure, (2012),

arXiv:1209.5743 (unpublished).

[29] T. Li, F. Becca, W. Hu and S. Sorella, Gapped spin-liquid phase in the J1-J2 Heisenberg model by a bosonic resonating valence-bond ansatz , Phys. Rev. B **86**, 075111 (2012).

Supplementary material

$|\Psi\rangle_{\mathbf{RVB}}$ has no AA (BB) pairing

In the main text, we have illustrated why the leading order contribution of NNN pairing vanishes in $|\Psi\rangle_{\mathrm{RVB}}$. Here we would like to show that, indeed, all the AA (BB) pairing vanish in $|\Psi\rangle_{\mathrm{RVB}}$ exactly up to any order in c. As explained in the text, the pairing amplitude between two sites i and j is given by the sum of all teleportation paths that connect i and j. As seen in Fig. 8, the solid red line a is a typical teleportation path that contributes to the pairing (ij). According to the local rule of the teleportation path (each path must turn at a vertex), it is not hard to see that any teleportation path contributing to the AA (BB) pairing must go through an odd number of corners and an even number of links. On the other hand, for a given teleportation path a, we can always find a dual teleportation path b which goes though the same number of corners and links. For any pair of dual a and b paths, the sign contribution from all the links (corners) are the same (opposite). Therefore, the total contribution from the pair of teleportation paths a and b always vanishes. Thus, we have proved that $|\Psi\rangle_{\mathrm{RVB}}$ has no AA (BB) pairing.

Finite size extrapolation of the optimum parameter c

We provide here a more accurate determination of the optimum parameter c. For this purpose, we use a quadratic function to fit the even sector ($|\Psi\rangle_e$) energy of a finite width (N_v) strip as a function of parameter c (around the minimum), and we extract the optimum parameter $c_{\mathrm{opt}}(N_v)$ and the minimum energy $E_{\mathrm{min}}(N_v)$ for $N_v = 10, \cdots, 24$. The results are presented in Fig. 9(a). Taking the optimum parameter $c_{\mathrm{opt}}(N_v)$ and extrapolating it to the thermodynamic limit as a function of inverse width $1/N_v$, we find $c_{\mathrm{opt}}(\infty) = 0.356(1)$ (see Fig. 9(b)). Again, taking the minimum finite width energy $E_{\mathrm{min}}(N_v)$ and extrapolating it to the thermodynamic limit as a function of $1/N_v$, we obtain a thermodynamic energy $E_\infty = -0.48620(1)$ (see Fig. 9(c)).
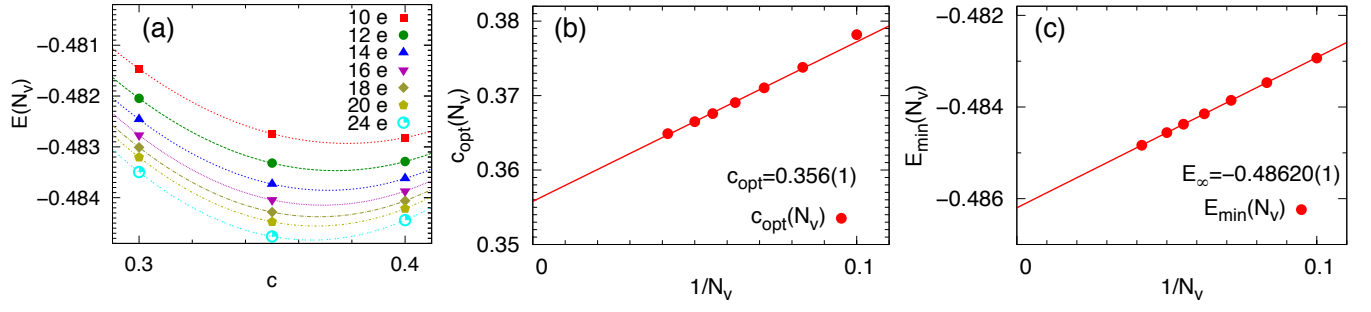
FIG. 9: (Color online)(a) A quadratic fit of the even sector energy $E(N_v)$ of a strip as a function of c around its minimum with $N_v = 10, \cdots, 24$. (b) Optimum parameter $c_{opt}(N_v)$ plotted as a function of $1/N_v$. A linear regression gives $c_{opt}(\infty) = 0.356(1)$. (c) Minimum energy $E_{min}(N_v)$ plotted as a function of $1/N_v$. A linear regression gives $E(\infty) = -0.48620(1)$.